The Response of the South Asian Summer Monsoon to Temporal and Spatial Variations in Absorbing Aerosol Radiative Forcing

Shao-Yi Lee and Chien Wang

GLOBAL CHANGE

MIT JOINT PROGRAM ON THE SCIENCE AND POLICY of GLOBAL CHANGE

GLOBAL CHANGE

MIT JOINT PROGRAM ON THE SCIENCE AND POLICY of GLOBAL CHANGE

*Reprinted with permission from

The Response of the South Asian Summer Monsoon to Temporal and Spatial Variations in Absorbing Aerosol Radiative Forcing

SHAO-YI LEE

Center for Environmental Sensing and Modeling, Singapore–MIT Alliance for Research and Technology, Singapore

CHIEN WANG

Center for Global Change Science, Massachusetts Institute of Technology, Cambridge, Massachusetts

ABSTRACT

Previous studies on the response of the South Asian summer monsoon to the direct radiative forcing caused by anthropogenic absorbing aerosols have emphasized the role of premonsoonal aerosol forcing. This study examines the roles of aerosol forcing in both pre- and postonset periods using the Community Earth System Model, version 1.0.4, with the Community Atmosphere Model, version 4. Simulations were perturbed by model-derived radiative forcing applied (i) only during the premonsoonal period (May–June), (ii) only during the monsoonal period (July–August), and (iii) throughout both periods. Soil water storage is found to retain the effects of premonsoonal forcing into succeeding months, resulting in monsoonal central India drying. Monsoonal forcing is found to dry all of India through local responses. Large-scale responses, such as the meridional rotation of monsoon jet during June and its weakening during July–August, are significant only when aerosol forcing is present throughout both premonsoonal and monsoonal periods. Monsoon responses to premonsoonal forcing by the model-derived "realistic" distribution versus a uniform wide-area distribution were compared. Both simulations exhibit central India drying in June. June precipitation over northwestern India (increase) and southwestern India (decrease) is significantly changed under realistic but not under wide-area forcing. Finally, the same aerosol forcing is found to dry or moisten the July–August period following the warm or cool phase of the simulations' ENSO-like internal variability. The selection of years used for analysis may affect the precipitation response obtained, but the overall effect seems to be an increase in rainfall variance over northwest and southwest India.

1. Introduction

The South Asian monsoon is a textbook monsoon system marked by a reversal of wind direction, from southward during winter to northward during summer, as the tropical convergence zone migrates from the Southern Hemisphere during winter to the Northern Hemisphere during summer. During the summer monsoon, a strong cross-equatorial flow is present over the Indian Ocean, accompanying a strong westerly lower-tropospheric jet over the Arabian Sea and supplying moisture to the subcontinent. High amounts of precipitation occur in this season, particularly over southwestern India as well as northeastern India where the monsoon flow meets orography.

In the past decade, there has been an increase in studies on the effects of anthropogenic aerosols on the South Asian summer monsoon because of concerns over the climate effects of the escalating abundance of anthropogenic aerosols over South Asia and surrounding regions. The persistent aerosol layer in the region, or the "atmospheric brown cloud," was found to contain a large quantity of absorbing aerosols or black carbon and cover a wide area of land and ocean (Ramanathan et al. 2001). Studies were thus conducted to examine whether the radiative effect of these absorbing aerosols could change the atmospheric radiative balance and thus alter the large-scale monsoonal circulation over the region. Menon et al. (2002), for example, found that the upper-level monsoon anticyclone over the Tibetan Plateau strengthens in response to a prescribed seasonally unvarying forcing representing absorbing aerosols, although it was difficult to determine the sign of rainfall

Corresponding author address: Lee Shao-Yi, Upper Air Observatory, 36 Kim Chuan Road, Singapore 537054, Singapore.
E-mail: lee_shao_yi@nea.gov.sg

change over India from their coarse-resolution model simulation.

The major atmospheric sink of aerosols is the scavenging of these particles by precipitation. Therefore, in the dry premonsoonal season before the coming of persistent monsoonal rainfalls [May–June (MJ)], aerosol abundance is much higher than during the actual monsoon season (June–September). The effect of aerosols in the premonsoonal period on these two phases of summer monsoon hence came to consideration. In a modeling study, Chung et al. (2002) applied direct radiative forcing during the premonsoon season to represent the effect of an atmospheric brown cloud. They found a weakening of the meridional temperature gradient resulting in a northward shift of the intertropical convergence zone (ITCZ), followed by a subsequent weakening of the June–July rainfall. Ramanathan et al. (2005) further expanded the above effort to include aerosol direct forcing throughout the whole year and identified a range of responses particularly in the monsoon season instead of the premonsoonal period, including weakened meridional sea surface temperature (SST) gradients, reduced evaporation, and increased atmospheric stabilization, all contributing to reduced rainfall particularly over central India. The weakening of the meridional sea surface temperature gradient leading to the weakening of the monsoon circulation (i.e., a large-scale response; Chung and Ramanathan 2006) is primarily caused by the surface cooling effects of aerosols and has thus become known as the "solar dimming effect." Using a coupled atmosphere and ocean general circulation model, Meehl et al. (2008) again demonstrated the role of the solar dimming effect during the monsoonal phase in weakening monsoonal circulation and precipitation. However, they also found that the effect from absorbing aerosols during the premonsoonal period enhances precipitation in certain areas such as northwestern India. Collier and Zhang (2009) found similar results of increased convection and precipitation over central India during the premonsoonal period and subsequent reduction during the monsoonal period.

Lau et al. (2006) described the transport and stacking up of anthropogenic absorbing aerosols against the slopes of the Tibetan Plateau particularly during the premonsoonal period, resulting in increased heating in elevated atmospheric layers above the slopes of the Tibetan Plateau by these aerosols. This "elevated heat pump" effect was later specified to dominate primarily in the northern regions of India during the premonsoon May–June period (Lau and Kim 2007, 2010). Randles and Ramaswamy (2008) have also found the effects from absorbing aerosols enhance the monsoon circulation and precipitation over northwestern India. Describing SST-mediated changes as slow responses and local atmospheric adjustments as fast responses, Ganguly et al. (2012a) found that the former was stronger overall, but the latter was dominant over northern regions of India, particularly northwestern India. However, neither study found a strong seasonality in the effects.

We have proposed in our previous studies that very localized aerosol forcing during the premonsoonal period—if placed at a sensitive position—is by itself capable of changing the stability of the lower atmosphere (in the format of a perturbation to the lower-tropospheric moist static energy) such as to create a positive feedback into the monsoon circulation. This results in a north-northwestward shift of precipitation pattern and enhances rainfall during the premonsoon period, particularly over northwestern India (Wang et al. 2009b; Lee et al. 2013). The pattern of precipitation change is similar to that revealed in Lau et al. (2006) as well as Meehl et al. (2008), without the need for transport and stacking of aerosols onto the slopes of the Tibetan Plateau.

Aerosol-induced responses could be multiple, and these effects would compete with each other given their complex nature; nonlinearity in response to different effects thus could arise in certain cases (e.g., Lee et al. 2013). Even varying the quantity of the same aerosols and hence relative forcing strength can lead to different climatic responses due to cloud radiative feedback (Randles and Ramaswamy 2008). Aerosol chemistry such as internal mixing and hygroscopic growth processes can change absorbing and scattering strength and the resultant atmospheric responses (Ming et al. 2005; Kim et al. 2008). Most of the previous studies have been about the effects of direct forcing of aerosols, partially because of the existence of anthropogenic absorbing aerosol or black carbon. However, indirect aerosol effects can also exert substantial influence on the monsoon system (Bollasina et al. 2011). Aerosols outside Asia can also have some influence on the monsoon response, although the dominant influence remains as a result of aerosols within the region (Ganguly et al. 2012b).

In this study, we use sensitivity simulations to address two issues that still linger regarding the direct radiative effect of anthropogenic absorbing aerosols on the South Asian summer monsoon climate. First, past studies of aerosol radiative effects on the South Asian summer monsoon have not assessed the relative contribution of aerosol forcing during the premonsoonal period against that during the monsoonal period, in terms of changes of circulation and precipitation as well as the mechanisms

responsible for these changes. It is true that aerosol radiative effects during the monsoonal period are much lower than those during the premonsoonal period because of the heavy precipitation scavenging of aerosols. Nevertheless, despite the scavenging by precipitation during the monsoonal period, aerosols still exist persistently because of the continuity in emissions (e.g., Wang et al. 2009a), and weak radiative forcing during the monsoonal period need not result in weak climate effects. Additionally, if the perturbation caused by aerosols during the premonsoonal period could propagate into the monsoonal period, then how substantial such an effect is compared to that of aerosol forcing during the monsoonal period needs to be examined, together with their mechanisms and their interaction.

Another issue that has not been addressed is the sensitivity of the aerosol-induced responses to the spatial distribution of aerosol radiative forcing. This study will examine whether the responses induced by aerosol effects in premonsoonal and monsoonal periods are sensitive to the spatial distribution of aerosol forcing.

In section 2 of this paper, details about our model simulations will be given on how different radiative forcing distributions and durations were applied over South Asia to highlight various mechanisms of aerosol direct effect. In section 3, simulations forced with "realistic" aerosol distributions during different phases of the monsoon will be compared, followed by the comparison of simulations with different spatial distributions of aerosol forcing in section 4. The interannual variability of precipitation response in various model simulations will be described in section 5. The conclusions are given in section 6.

2. Methodology

a. Model and configuration

The model used in this study is the Community Earth System Model (CESM), version 1.0.4 (Gent et al. 2011). The fully coupled configuration (B preset) was adopted, which includes component models for ocean [Parallel Ocean Program, version 2 (POP2)], atmosphere [Community Atmosphere Model, version 4 (CAM4)], land [Community Land Model, version 4 (CLM4)], and land ice as well as sea ice [Community Ice Sheet Model (CISM) and Community Ice Code, version 4 (CICE4)], all in prognostic mode. Although the fully coupled configuration is much more computationally demanding compared to the one using prescribed SST, previous work has indicated that inclusion of ocean feedback to the atmosphere is important for capturing accurate climate responses to aerosol forcing (Wang 2007). The atmosphere and land

models were run on the $1.9° \times 2.5°$ latitude–longitude grid, and the ocean model and the ice model were run at a $1°$ horizontal resolution (gx1v6). All the component models were evolved freely under the year-2000 anthropogenic forcing given in the model except for aerosol forcing. To isolate the climate responses to anthropogenic aerosols, the radiative effects of natural aerosols (dust and sea salt) were excluded. Six simulations were carried out as described below (and listed in Table A1).

The control simulation was the no-aerosol climate (B2000NOAER), which was integrated for 240 years. The simulation approached equilibrium climate rapidly in about 60 years, and the last 100 years were used in analysis.

For two simulations, the direct radiative forcing of anthropogenic absorbing aerosols was prescribed over an area in the rather idealized shape shown in Figs. 1a,b, either during the premonsoonal period from May to June (BOCEANHF-PRE) or during the monsoonal period from July to August (BOCEANHF-MON). These simulations are termed wide-area simulations. In comparison to our previous study with a localized premonsoonal forcing, which was designed to test the monsoon response to aerosol forcing at one specific sensitive location (dark gray shaded region of Fig. 1c; Lee et al. 2013), the wide-area simulations in this study were forced over a larger area covering both land and ocean. Note that we do not consider this spatial distribution to be very realistic but have designed it in order to understand how aerosol forcing over the ocean, in particular over the Arabian Sea, influenced the monsoon response in early studies (e.g., Chung et al. 2002). Hence, we excluded forcing over East Asia and Indo-China regions to introduce a spherical spatial forcing covering the Arabian Sea and the western side of South Asia. The strength of the aerosol forcing was also reduced from Chung et al. (2002), which was used as our reference, of approximately $-30\,\mathrm{W\,m^{-2}}$ for surface and $20\,\mathrm{W\,m^{-2}}$ for atmospheric forcing $[-10\,\mathrm{W\,m^{-2}}$ at the top of atmosphere (TOA)] over the Arabian Sea. We reduced these values to $-10\,\mathrm{W\,m^{-2}}$ at the surface and $8\,\mathrm{W\,m^{-2}}$ in the atmosphere (about $1\,\mathrm{K\,day^{-1}}$ in the lowest three model layers of the terrain-following vertical coordinates to approximately $925\,\mathrm{hPa}$) or $-2\,\mathrm{W\,m^{-2}}$ at TOA. These values make the forcings comparable to the prescribed forcings used in our other simulations and to reduce the effect of discontinuity in the forcing when prescribed in certain months. Both of these idealized simulations were integrated for 200 years, and the last 100 years was used in analysis.

The shortwave forcing of anthropogenic absorbing aerosols used in the other three realistic simulations was derived from a previous interactive aerosol model simulation (Kim et al. 2008). The monthly climatology of the radiative effect of anthropogenic absorbing components
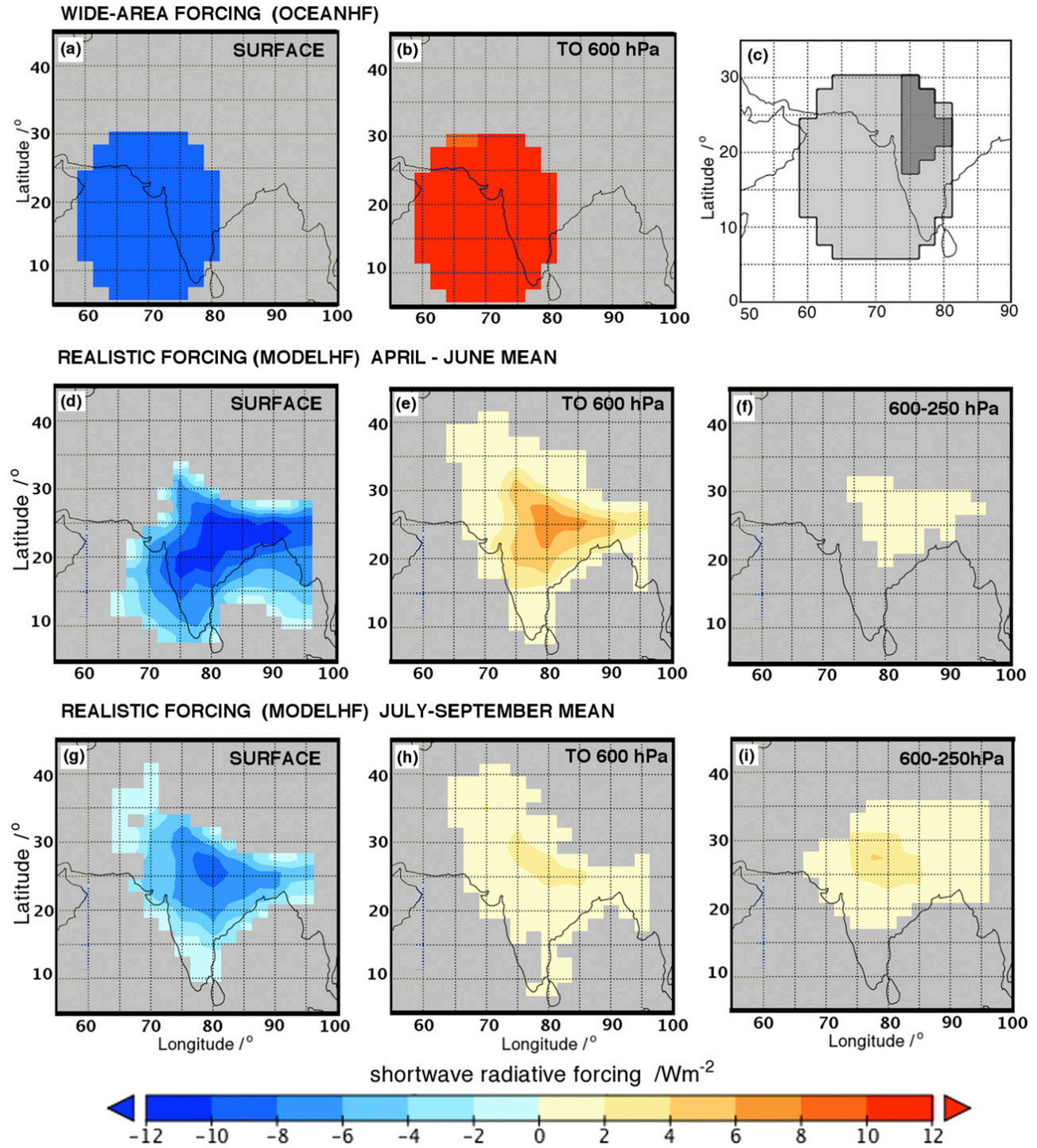
FIG. 1. Prescribed shortwave radiative forcing (W m^{-2}) in perturbed simulations. Forcing in the idealized wide-area simulations at the (a) surface and (b) lower troposphere. (c) Comparison of the coverage of wide-area simulations with the localized forcing in a previous study (Lee et al. 2013). The mean forcing from April to June at (d) the surface, (e) the lower troposphere, and (f) the upper troposphere. (g)–(i) As in (d)–(f), but showing the mean forcing from July to September. Note that the forcing is different for every month.

was used (i.e., that of external black carbon and the internal mixture with sulfate shell and black carbon core). In calculating these values, feedbacks from the aerosol forcing to the modeled climate were switched off (i.e.,

"offline mode"; cf. Wang 2004; Kim et al. 2008). Only the shortwave forcing of aerosols was considered in this study, and the radiative forcing was applied only during the daytime, scaled by the solar zenith angle. The realistic
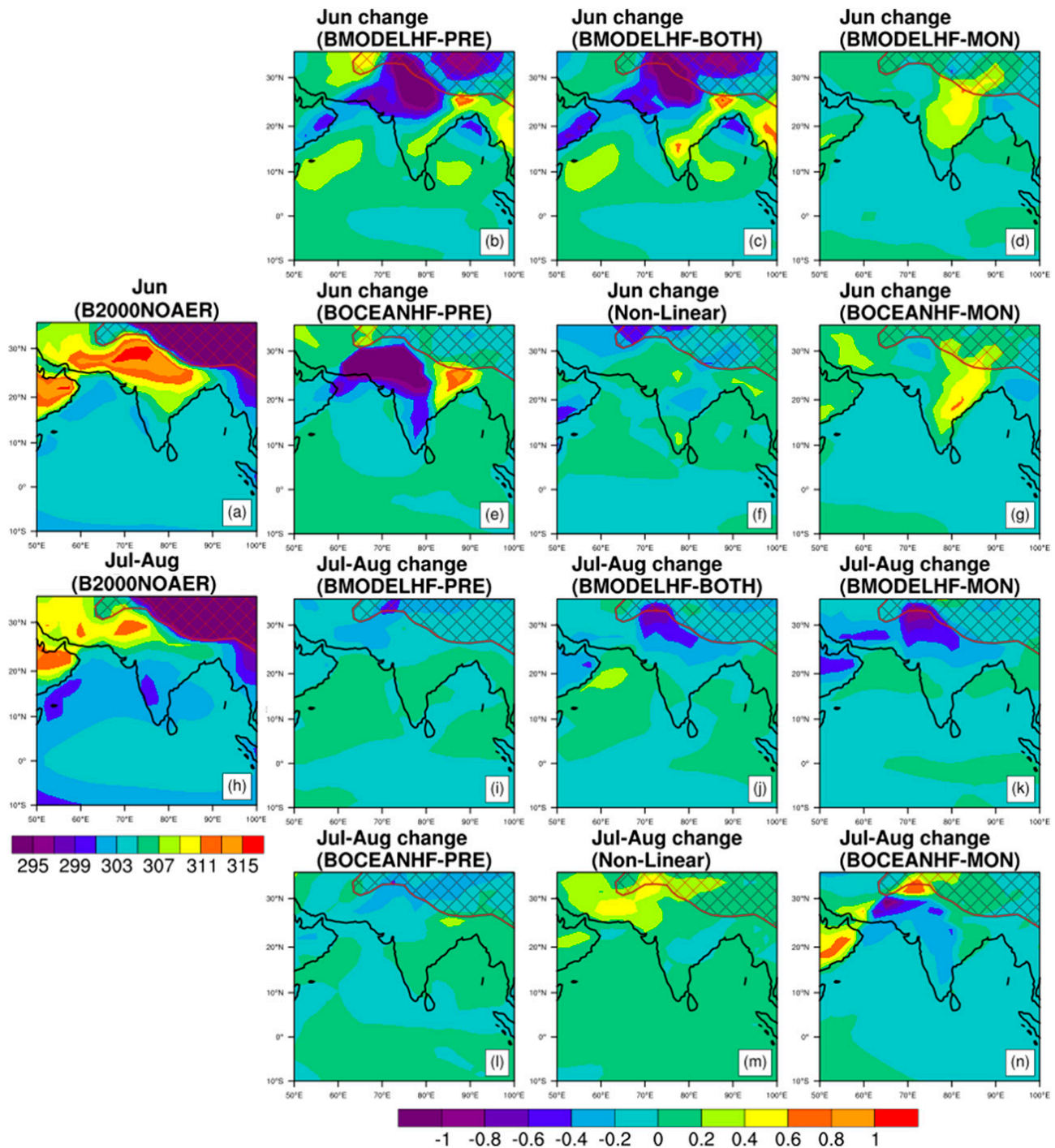
FIG. 2. Surface temperature in the control and changes in perturbed models (K). (a) Mean June surface temperature in the control simulation. Changes in mean June surface temperature for the (b) realistic premonsoonal, (c) both-period, and (d) monsoonal simulations as well as for the (e) wide-area premonsoonal and (g) monsoonal simulations. (f) Nonlinear contribution to the changes in realistic both-period simulation. (h)–(n) As in (a)–(g), but for July and August. Regions higher than 1.5 km (~850 hPa) are hatched.

forcing was more localized over land than the idealized forcing, although both included negative surface forcing over the ocean (Figs. 2e–h). In addition, sources of upper-tropospheric heating of absolute value up to $+4 \, W \, m^{-2}$ exist in the model-derived profile particularly during the

monsoonal period (Figs. 2f,i) because of convective transport of aerosol species up to 100 hPa (Kim et al. 2008). Note that the direct radiative effects of anthropogenic absorbing aerosols considered in this study still contain a scattering component besides an absorbing one,

particularly coming from the core-shell internal mixture of black carbon and sulfate.

The three above-mentioned simulations were forced respectively during the premonsoonal period from April to June only (BMODELHF-PRE, Figs. 1d–f), during the monsoonal period from July to September only (BMODELHF-MON, Figs. 1g–i), and during both periods from April to September (BMODELHF-BOTH). It was observed that when realistic aerosol forcing was prescribed only for two months, the model took a much longer time to approach equilibrium climate in comparison to the idealized simulations. When the prescribed forcing was slowly increased from its April value to its June value, the time to reach equilibrium climate was reduced. The realistic simulations were integrated for 240 years, and the last 140 years were used for analysis. These simulations were considered to have

approached equilibrium by 100 years since the climatology is qualitatively similar whether calculated using the last 100 years or 140 years, despite having certain transient features.

b. Model diagnostics

When analyzing the model results, the climate response of a given climate parameter to a given prescribed aerosol forcing was derived by

$$\text{response(forced simulation)} = \text{results(forced simulation)} - \text{results(control)}.$$

The response of the realistic forcing simulation during both premonsoonal and monsoonal periods can be partitioned as

$$\text{response(both period forcing)} = \text{response(premonsoonal forcing)} + \text{response(monsoonal forcing)} + \text{nonlinear component}.$$

The nonlinear component can be considered indicative of feedback processes when the climate responses of premonsoonal and monsoonal forcing interact with each other.

As a guide to whether the climate response of the model to aerosol radiative forcing could be attributed in observations when compared to other sources of climate variability, a number of diagnostics for the monsoon system were calculated (see appendix, section a), and changes in their distribution functions were tested for statistical significance (see appendix, section b). With regard to deterministic models, the lack of statistical significance in the climatic response to perturbations does not mean that there is no response but that the response is small. Indeed, similar changes in climate responses occur in our simulations that only differ in their strength, despite the responses being statistically significant in one and not the other.

3. Equilibrium climate under realistic forcing: The roles of premonsoonal and monsoonal forcing

a. Forcing applied only during the premonsoonal and onset period

The equilibrium climate under realistic aerosol forcing only during the premonsoonal period (BMODELHF-PRE) showed significant reductions in the premonsoonal interhemispheric surface temperature gradient (Table 1,

row a; Fig. 2b), monsoon jet transport of water vapor (Table 1, row b; Fig. 3b), and all-India total precipitation (Table 1, row e; Fig. 4b). Note that the precipitation change was not uniform over India. June precipitation decreased only over central and southwestern India (Table 1, rows f and g). Over northwestern India, it increased instead (Table 1, row h). During the monsoonal period [i.e., July–August (JA)] most of the climate diagnostics in the simulation with only realistic premonsoonal forcing were not significantly changed (Table 1, rows i–o). The exception was a reduction in precipitation over central India (Table 1, row m; Fig. 4i).

To better understand the processes behind the precipitation changes, we have compared changes in precipitation over the different subregions of India against changes in the horizontal convergence of water vapor fluxes vertically integrated over the lower troposphere, as well as water vapor exchange between the atmosphere and Earth's surface, termed "surface water flux." During the month of June, the convergence of horizontal water vapor flux over central India significantly decreased (Table 2, row a). Together with the decrease in jet transport and central India precipitation, this result was consistent with the solar dimming mechanism, at least during June. Nevertheless, there is some distinction in the exact mechanism involved. For instance, we might expect reduced horizontal water vapor convergence over southwestern India as well should solar dimming, in the sense of SST-mediated circulation, be

TABLE 1. Changes in monsoon diagnostics (see appendix, section a; Table A2), comparing distributions of 20-yr climates from forced simulations with the distribution from the control simulation (see appendix, section a; Table A1). Boldface, lightface, and italic text describe changes from the control significant at the 99%, 95%, and 90% confidence level, respectively (see appendix, section b). Empty cells indicate no significant changes. Asterisks mark results not accounted for by changes of either water vapor flux convergence or surface water flux (cf. Tables 2 and 3). The period for which a variable is calculated appears in the square brackets following the variable.

		Premonsoonal forcing			Monsoonal forcing	
	Diagnostic	BOCEANHF-PRE	BMODELHF-PRE	BMODELHF-BOTH	BMODELHF-MON	BOCEANHF-MON
A	TSDIFF[MJ]	**Decrease**	**Decrease**	**Decrease**		
B	JETSTR[Jun]	Decrease	**Decrease**	**Decrease**		
C	JETANG[Jun]			**Decrease**		
E	ALL_PRECT[Jun]	Decrease	**Decrease**	**Decrease**		*Decrease*
F	CTR_PRECT[Jun]	Decrease	**Decrease**	**Decrease**		*Decrease*
G	SW_PRECT[Jun]		*Decrease*	**Decrease**		
H	NW_PRECT[Jun]		**Increase**	**Increase**		
I	JETSTR[JA]			*Decrease*		*Decrease*
j	JETANG[JA]				*Increase*	*Decrease*
l	ALL_PRECT[JA]			**Decrease**	*Decrease*	**Decrease**
m	CTR_PRECT[JA]		*Decrease*	**Decrease**	**Decrease**	**Decrease**
n	SW_PRECT[JA]				*Decrease*	*Decrease*
o	NW_PRECT[JA]			**Decrease**	*Decrease**	**Decrease**

responsible. However, the reduction of total precipitation over southwestern India was not so much a result of the weakened jet transport causing less horizontal water vapor convergence over the subregion (Table 2, row c) but more a result of reduced evaporation over the Arabian Sea (Table 2, row d). There are multiple causes for reduced evaporation, including directly by reduced insolation as a result of aerosol forcing, indirectly by the weakened surface winds (see Fig. 7b), and by the slightly cooled surface (Fig. 2b), all of which would slow evaporation. Note that since most of the precipitation over southwestern India fell over the ocean in the model, our region of analysis thus included these ocean regions (see appendix, section a). In reality, the precipitation has been observed to concentrate over the Western Ghats mountain range along the coast of southwestern India.

Over northwestern India, both horizontal water vapor convergence and surface water flux during June significantly increased (Table 2, rows e and f), and their absolute quantities were similar. But unlike the southwest subregion that contains large areas of ocean, the northwest subregion contains only land. In addition, the preceding months were arid and would limit soil water availability in the northwest subregion. Thus, the increase in surface water flux should be more a consequence of increased precipitation than the reverse. This leaves the increased convergence as the primary reason for increased precipitation. The precipitation increase over northwestern India is consistent with previous results (e.g., Meehl et al. 2008; Wang et al. 2009b; Lee et al. 2013; see also the introduction), and we will discuss the details of this increase further in section 4a.

During the monsoonal period, the reduction in precipitation over central India was primarily due to a reduction of surface water flux (Table 3, row b). Surprisingly, reduced soil moisture over central India from a drier June persisted into July (see Fig. 9). This suggests that over central India, the land surface helps to transmit the drying effects of premonsoonal aerosol forcing into the monsoon season by limiting evaporation.

b. Forcing applied only during the monsoonal period

The equilibrium climate under realistic aerosol forcing only during the monsoonal period (BMODELHF-MON) did not display any significant change in the climate diagnostics during June (Table 1, rows a–h). However, during July and August, total precipitation significantly decreased over all three subregions of India (Table 1, rows m–o). Water vapor transport by the monsoon jet was not significantly changed (Table 1, row i), but the direction of the jet was rotated clockwise to a much more eastward orientation (Table 1, row j).

Reduced central and southwestern India precipitation was concurrent with decreases of horizontal water vapor convergence and surface water flux over the two subregions (Table 3, rows a–d). The change in precipitation over southwestern India was weak (see Fig. 7g), and thus we focus on the central India pattern in our discussion (Fig. 4k). Aerosol-induced surface cooling over central India (Fig. 2k) reduces surface water flux over land (Table 3, rows a–d), which results in decreased precipitation during the monsoonal period. The decreased precipitation reduces soil water (Fig. 5k), which would
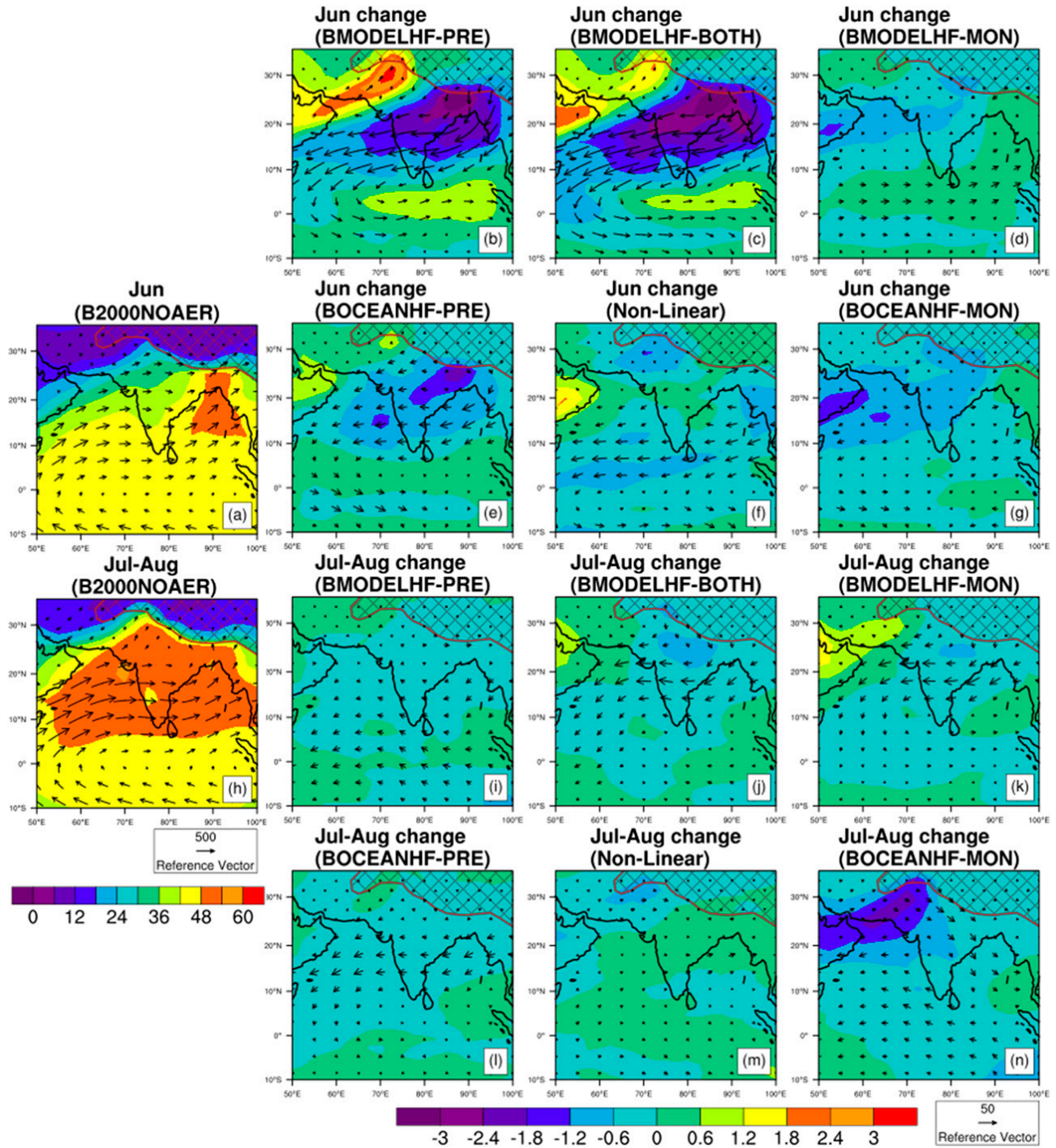
FIG. 3. As in Fig. 2, but showing water vapor vertically integrated over the lower troposphere (kg m^{-2}), or up to approximately 570 hPa. Vectors show horizontal water vapor flux vertically integrated over the lower troposphere (kg m^{-1} s^{-1}).

further suppress surface flux. Interestingly, except for the precipitation reduction over central India, many features of aerosol-induced changes could not be simply explained by aerosol solar dimming effect. There is no significant reduction in the amount of water vapor transported into the monsoon system such that large-scale circulation was weakened. Instead, the main reason

appears to be as a result of local responses in stability and evaporation. The directional rotation of the monsoon jet may have additional effects.

Over northwestern India, July–August precipitation was significantly reduced, yet neither the convergence of horizontal water vapor flux nor surface water fluxes were significantly changed (Table 3, rows e and f). The
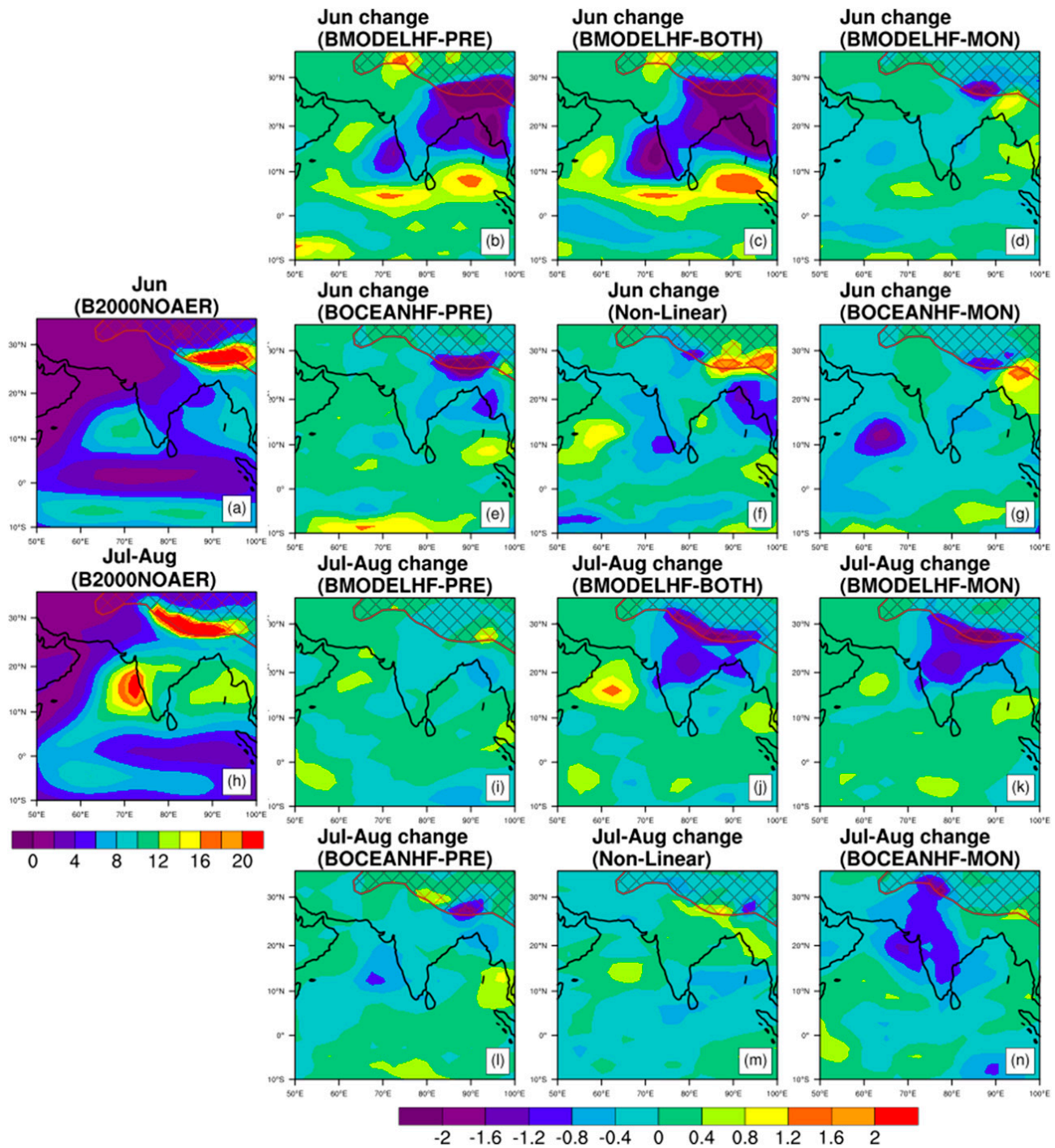
FIG. 4. As in Fig. 2, but showing total precipitation (mm day^{-1}).

climatological means of precipitation, the convergence of horizontal water vapor flux, and surface water flux were all lower than the values in the control case, but the differences are not statistically significant. A clockwise rotation of the monsoon jet to a more zonal orientation was observed, which would reduce the northward flux of water vapor. (Table 1, row j; also cf. section 4a).

c. Forcing applied throughout both premonsoonal and monsoonal periods

The equilibrium climate of June under realistic forcing applied in both premonsoonal and monsoonal periods (BMODELHF-BOTH) resembled that of the realistic premonsoonal forcing simulation. Compared to

TABLE 2. As in Table 1, but showing June changes in regional diagnostics of precipitation taken from Table 3, rows c and d, compared to changes in regional diagnostics of water vapor flux convergence (QCONV) and surface water vapor flux (QSFC). Boldface, lightface, and italic text describe changes from the control significant at the 99%, 95%, and 90% confidence level, respectively. Empty cells indicate no significant changes.

| | Diagnostic | Premonsoonal forcing | | | Monsoonal forcing | |
		BOCEANHF-PRE	BMODELHF-PRE	BMODELHF-BOTH	BMODELHF-MON	BOCEANHF-MON
	CTR_PRECT[Jun]	Decrease	**Decrease**	**Decrease**		Decrease
a	CTR_QCONV[Jun]	Decrease	**Decrease**	**Decrease**		
b	CTR_QSFC[Jun]	**Decrease**	**Decrease**	**Decrease**		**Decrease**
	SW_PRECT[Jun]		*Decrease*	**Decrease**		
c	SW_QCONV[Jun]	Increase		*Decrease*		
d	SW_QSFC[Jun]	**Decrease**	**Decrease**	**Decrease**		
	NW_PRECT[Jun]		**Increase**	**Increase**		
e	NW_QCONV[Jun]		Increase			
f	NW_QSFC[Jun]		**Increase**	**Increase**		

the control simulation, the May–June interhemispheric surface temperature gradient (Table 1, row a; Fig. 2c) and the monsoon jet transport of water vapor (Table 1, row b; Fig. 3c) were both reduced. Total precipitation decreased over central and southwestern India (Table 1, rows f and g) but increased over northwestern India (Table 1, row h). The pattern of precipitation change was similar to that of the premonsoonal simulation from the control (Fig. 4b versus Fig. 4c).

During July and August, however, the equilibrium climate mostly resembled that of the realistic monsoonal forcing simulation (Figs. 2c, 3c, 4c, 5c, and 6c versus Figs. 2d, 3d, 4d, 5d, and 6d). Precipitation in central and northwestern India was significantly reduced in both simulations (Table 1, rows m and o). The difference in southwestern India precipitation between both-period-forcing and monsoonal-forcing simulations (Table 1, row n) was due to increased precipitation over the Arabian Sea, while at the coastal region the patterns and magnitudes of precipitation reduction were almost the same in the both-period-forcing and monsoonal-forcing simulations (Fig. 4j versus Fig. 4k). The monsoon jet transport of water vapor was significantly weakened in

the both-period simulation (Table 1, row i) unlike in the monsoonal-forcing simulation where it was not significantly changed. Differing from the result for June, there was no obvious monotonic relationship between the strength of the July–August jet transport in the different models, and the premonsoonal interhemispheric surface temperature gradient (Fig. 7a versus Fig. 7e).

To identify the interplay between the responses respectively induced by aerosol forcing in the premonsoon and monsoon period, we first examine whether the presence of monsoonal forcing could alter the precipitation response to premonsoonal forcing during June. The June climate of the both-period simulation was drier over all subregions compared to the premonsoonal-forcing simulation, although forcing during the premonsoonal season was the same in both-period-forcing and premonsoonal-forcing simulations (Figs. 7b–d). The dryness was not due to a linear addition of precipitation responses to monsoonal and premonsoonal forcing, but rather a nonlinear effect to the precipitation rising from these two forcing components; the extent of the nonlinear contribution to precipitation change is actually larger than that obtained in the

TABLE 3. As in Table 2, but for July–August. Asterisks mark results where precipitation change is accounted for by neither changes in convergence of horizontal water vapor flux nor surface water flux.

| | Diagnostic | Premonsoonal forcing | | | Monsoonal forcing | |
		BOCEANHF-PRE	BMODELHF-PRE	BMODELHF-BOTH	BMODELHF-MON	BOCEANHF-MON
	CTR_PRECT[JA]		*Decrease*	**Decrease**	**Decrease**	**Decrease**
a	CTR_QCONV[JA]			**Decrease**	**Decrease**	Decrease
b	CTR_QSFC[JA]		*Decrease*	**Decrease**	**Decrease**	**Decrease**
	SW_PRECT[JA]				*Decrease*	*Decrease*
c	SW_QCONV[JA]				*Decrease*	*Decrease*
d	SW_QSFC[JA]	**Decrease**		**Decrease**	**Decrease**	**Decrease**
	NW_PRECT[JA]			**Decrease**	*Decrease**	**Decrease**
e	NW_QCONV[JA]			*Decrease*	*	**Decrease**
f	NW_QSFC[JA]		*Increase*		*	**Decrease**
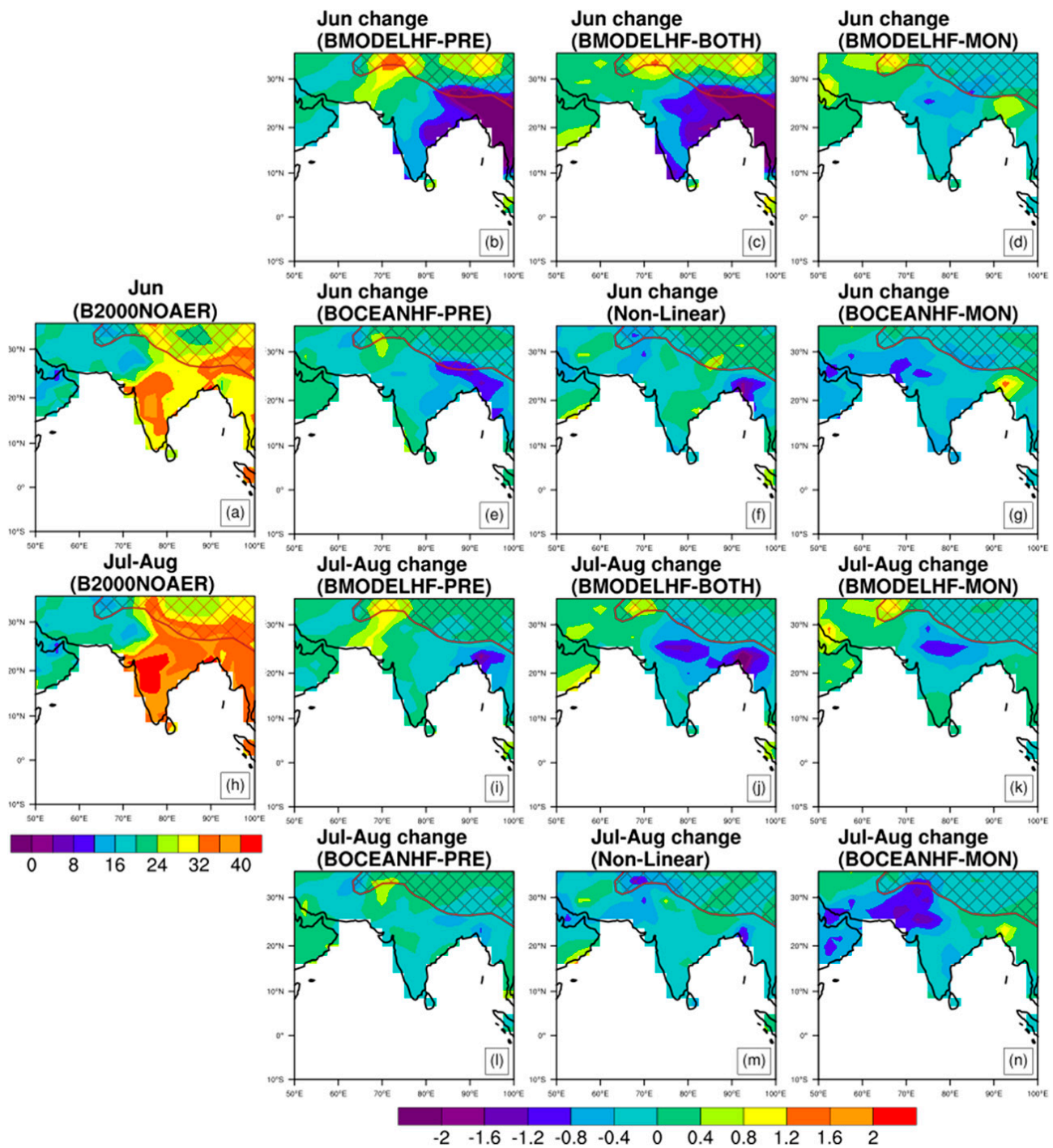
FIG. 5. As in Fig. 2, but showing soil water vertically integrated over the first 1 m of soil (cm).

monsoonal-forcing simulation (Fig. 4f versus Fig. 4d). This consists of a reduction of precipitation on the east side of the Arabian Sea as well as off the west coast of the Indian subcontinent, and an increase in precipitation on the west side of the Arabian Sea. The nonlinear precipitation response can be attributed to water vapor distribution; in the lower troposphere, easterly water flux

anomalies over the Arabian Sea and a zonal shift in column water vapor distribution toward the west can be seen in the distribution of nonlinear components (Fig. 3f).

Regarding temperature change, premonsoonal forcing weakened not only the June meridional surface temperature gradient (section 3a) but also the zonal temperature gradient between the Arabian Sea and the Indian
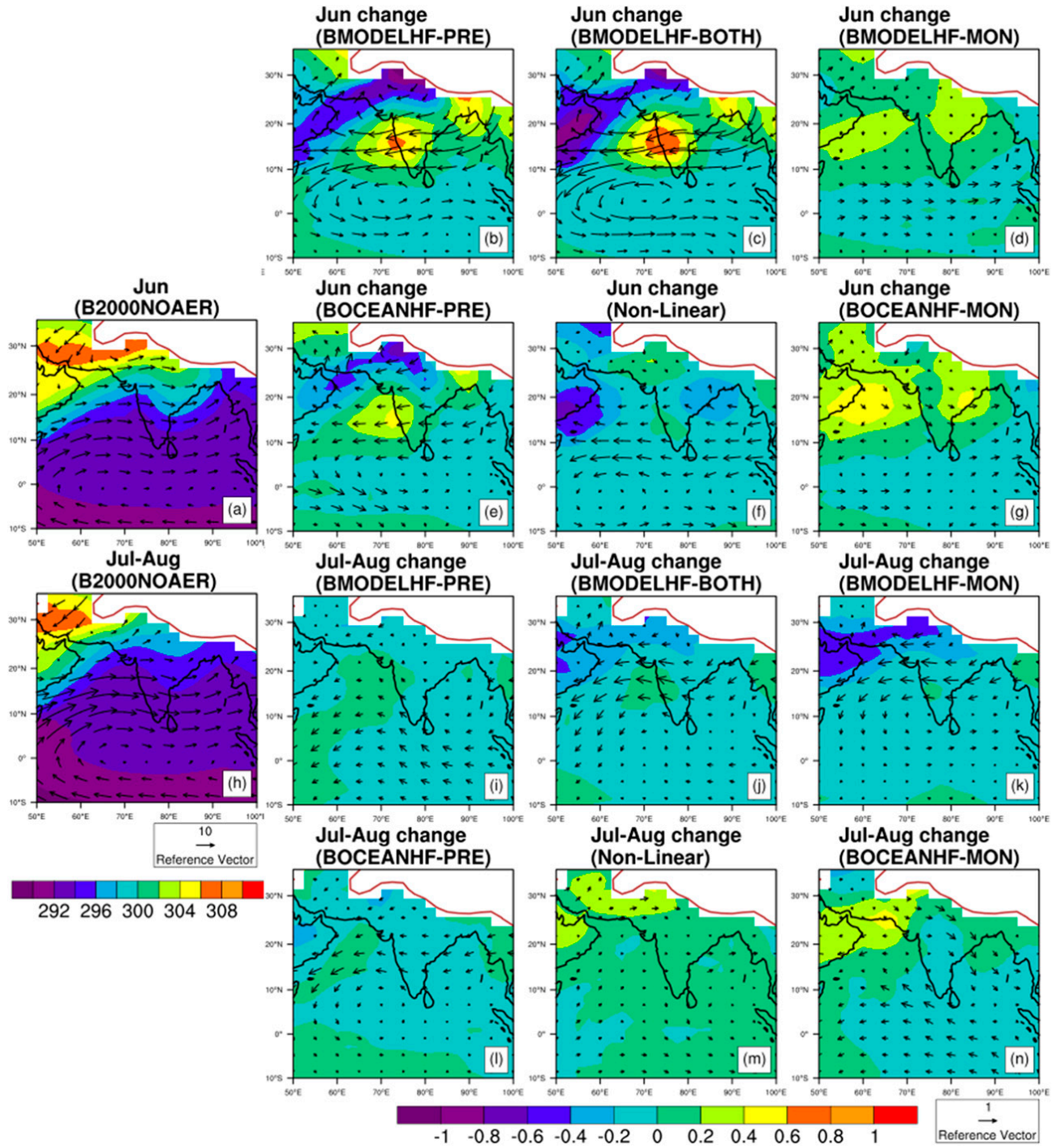
FIG. 6. As in Fig. 3, but showing temperature (K) at 850 hPa. Vectors show wind (m s^{-1}) at 850 hPa. White region outlined by the red contour is underground.

subcontinent (Figs. 2a,b). When monsoonal forcing was added, there was greater weakening of the zonal gradient (Figs. 2a,c). However, surface temperature change in the both-period-forcing simulation (Fig. 2c) was a mostly linear addition of the respective responses to premonsoonal and to monsoonal forcing (Figs. 2d,b).

On the other hand, above the surface, the same weakening of horizontal temperature gradients was observed in the lower troposphere (Figs. 6a,c). But unlike at the surface, a strong nonlinear component reinforced the zonal dipole temperature anomaly across the Arabian Sea (Fig. 6f). The anomalous warm–cool–warm zonal
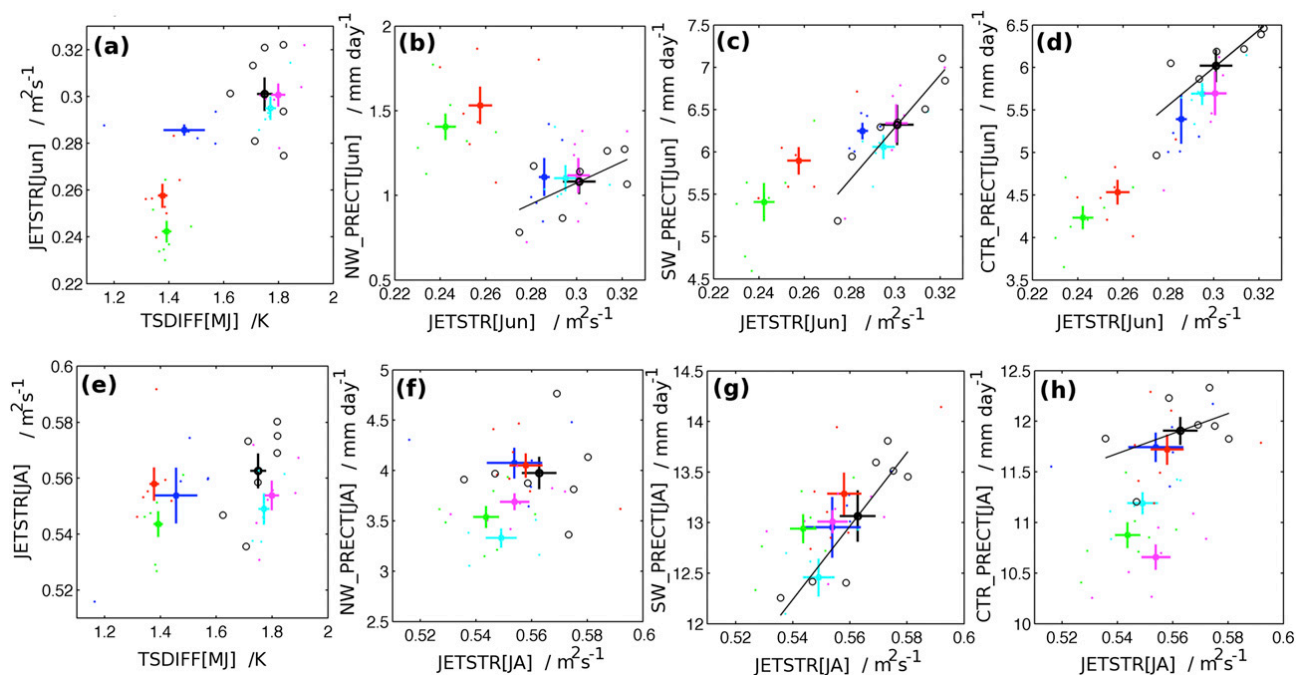
FIG. 7. Scatterplots of climate diagnostics as displayed on the axis labels. (a) JETSTR[Jun] vs TSDIFF[MJ]. (b)–(d) NW_PRECT[Jun], SW_PRECT[Jun], and CTR_PRECT[Jun], respectively, vs JETSTR[Jun]. (e)–(h) As in (a)–(d), but for JETSTR[JA] and monthly mean total precipitation (PRECT) during JA. Colored crosses show the mean of the 20-yr climates, and the length of the bars of crosses shows the standard deviation of the mean. The models are as follows: B2000NOAER (black), BMODELHF-PRE (red), BMODELHF-MON (magenta), BMODELHF-BOTH (green), BOCEANHF-PRE (blue), and BOCEANHF-MON (cyan). Black circles and colored dots mark values of individual 20-yr climates. For the control simulation, a black line is drawn showing the linear fit to the 20-yr climates if there is a statistically significant nonzero slope. Note that tick marks are the same for the same type of diagnostics, although the ranges are different in different plots.

structure of the nonlinear temperature response corresponded to the anomalous wet–dry–wet structure of the nonlinear precipitation response (Fig. 4f). Thus, the nonlinear response is due to the feedback between the temperature response to precipitation changes (i.e., evaporative cooling of precipitation) and the precipitation response to temperature changes (i.e., through water vapor redistribution). However, mechanisms are still needed to propagate the effects of aerosol forcing during the monsoonal period to the start of the next summer monsoon season.

Similar to the above analysis, there was weak warming associated with reduced precipitation during June in the monsoonal-forcing simulation, although there was no forcing during June (Figs. 4d and 6d). In this simulation, the warm surface temperature anomaly over central India during June is consistent with the idea of reduced evaporative cooling at the ground (Fig. 2d). Reduced soil moisture over central India in the both-period-forcing simulation mostly reflects a linear addition of soil moisture changes in the monsoonal-forcing simulation and premonsoonal simulation (Figs. 5b–d).

Thus, soil moisture surprisingly retained the effect of monsoonal-period forcing into the following June

(Fig. 5d), and it could be a mechanism that propagates the effect of aerosol forcing during the monsoonal period to the start of the next summer monsoon season. We suggest that changes in the soil moisture limit precipitation during the critical period of June, when advective sources of water vapor are still limited. This minor change in precipitation is sufficient to alter temperature gradients, resulting in wind and water vapor flux anomalies, which in turn lead to a larger change in precipitation that reinforces the precipitation changes caused by premonsoonal forcing.

We next consider whether the presence of premonsoonal forcing can alter the precipitation response to monsoonal forcing during July and August. When premonsoonal forcing was applied prior to the forcing during the monsoonal period, the distribution of column water vapor in the lower troposphere was changed (shading, Fig. 3m), resulting in weaker horizontal gradient changes (Fig. 3j versus Fig. 3k). In the nonlinear component, the resultant effect could reduce precipitation over northwestern India (Fig. 4m), resulting in lower soil moisture (Fig. 5m), warming at the surface and lower troposphere (Figs. 2m and 6m) resulting from less evaporative cooling, and, to close the cycle, reduced

column water vapor. This is a negative feedback to the effect of premonsoonal forcing and prevents excessive surface cooling in the west side of the Arabian Sea (Fig. 2i) or the zonal temperature gradient from weakening further. Thus, the effects of premonsoonal forcing on the monsoonal period were limited by the above negative feedback.

4. Comparison between equilibrium climates under realistic and idealized forcing

a. Applying forcing during the premonsoonal and onset period

To further clarify the climate response to premonsoonal aerosol forcing, we have compared the response in the realistic premonsoonal-forcing simulation (BMODELHF-PRE) to that in the idealized, or wide-area, premonsoonal-forcing simulation (BOCEANHF-PRE).

Despite differing in magnitude, the changes in the equilibrium premonsoonal climate derived from these two simulations from that of the control simulation were generally similar (Figs. 2b, 3b, 4b, 5b, and 6b versus Figs. 2e, 3e, 4e, 5e, and 6e). Both simulations showed significant reductions of May–June interhemispheric surface temperature gradients (Table 1, row a), June jet transport of water vapor (Table 1, row b), and all-India precipitation (Table 1, row e). Unlike in the realistic simulation, total precipitation over southwestern and northwestern India was not significantly reduced in the wide-area simulation. Regionally, the pattern of precipitation anomaly was largely similar over southwestern India from the realistic and wide-area simulations while it differed over northwestern India, and hence we focus our discussion on the latter.

The largest difference between the precipitation response in the wide-area and the realistic simulations was seen over northwestern India. The change in column water vapor gradient and accompanying increase in precipitation over northwestern India were absent in the wide-area simulation (Fig. 3e versus Fig. 3b).

In our previous study where highly localized shortwave forcing was prescribed over an inland region during the premonsoonal period, both the water vapor transport by the monsoon jet and total precipitation over northwestern India were found to strongly increase in June (Lee et al. 2013). The difference between the current wide-area (jet weakened) and previous localized (jet strengthened) simulations suggests that aerosol-induced perturbation to the monsoon jet in June is sensitive to the spatial distribution of the forcing. In addition, comparison between the current realistic (jet

weakened) and previous localized (jet strengthened) simulations also indicates that such a perturbation to the monsoon jet in June is sensitive to forcing over the ocean as well.

Two reasons have been found to cause the increase of precipitation over northwestern India derived in the previous study. First, a local anticyclonic anomaly over the Indian subcontinent could have brought more water vapor into northwestern India, changing atmospheric stability and shifting convection northward. Second, a stronger monsoon jet could have increased the amount of water vapor entering the monsoon system. The former process can be regarded as a local change internal to the monsoon system while the latter a large-scale change of the monsoon system.

In addition to these two processes, we now find that the monsoon jet itself can rotate anticlockwise toward a more northward orientation, bringing more water vapor flux into northwestern India with the same effect as the above-mentioned first process. During June, anticlockwise rotation of the monsoon jet by 1.2° was observed in the realistic premonsoonal simulation, but only 0.3° was observed in the wide-area premonsoonal simulation (Fig. 3e versus Fig. 3b).

b. Applying forcing during the monsoonal period

Wide-area radiative forcing during the monsoonal period was an unrealistic scenario, but we still performed a comparison between the climatic responses to wide-area and realistic monsoonal forcing to gain scientific understanding. An idealized simulation as in Lee et al. (2013) with localized aerosol distribution was not performed because the spatial distribution of the realistic forcing was so similar to the localized idealization that we believe the changes between the two would be small compared to the computational demand required.

The wide-area monsoonal forcing is found to significantly reduce June precipitation over central India in the premonsoonal period (Table 1, row f). Significant reduction in surface water flux is also seen over central India (Table 2, row b). The realistic simulation did not produce such significant changes only because there was a larger variability in the climatology (Figs. 8a,b).

The stronger persistent effect in the wide-area simulation compared to the realistic simulation is apparently due to the more widespread forcing during the monsoonal period. During the monsoonal period, large regions on the north and east side of the Arabian Sea as well as the Arabian Peninsula experienced reduction in precipitation in the wide-area simulation compared to the realistic simulation (Fig. 4n versus Fig. 4k). Soil moisture was accordingly reduced (Fig. 5n versus
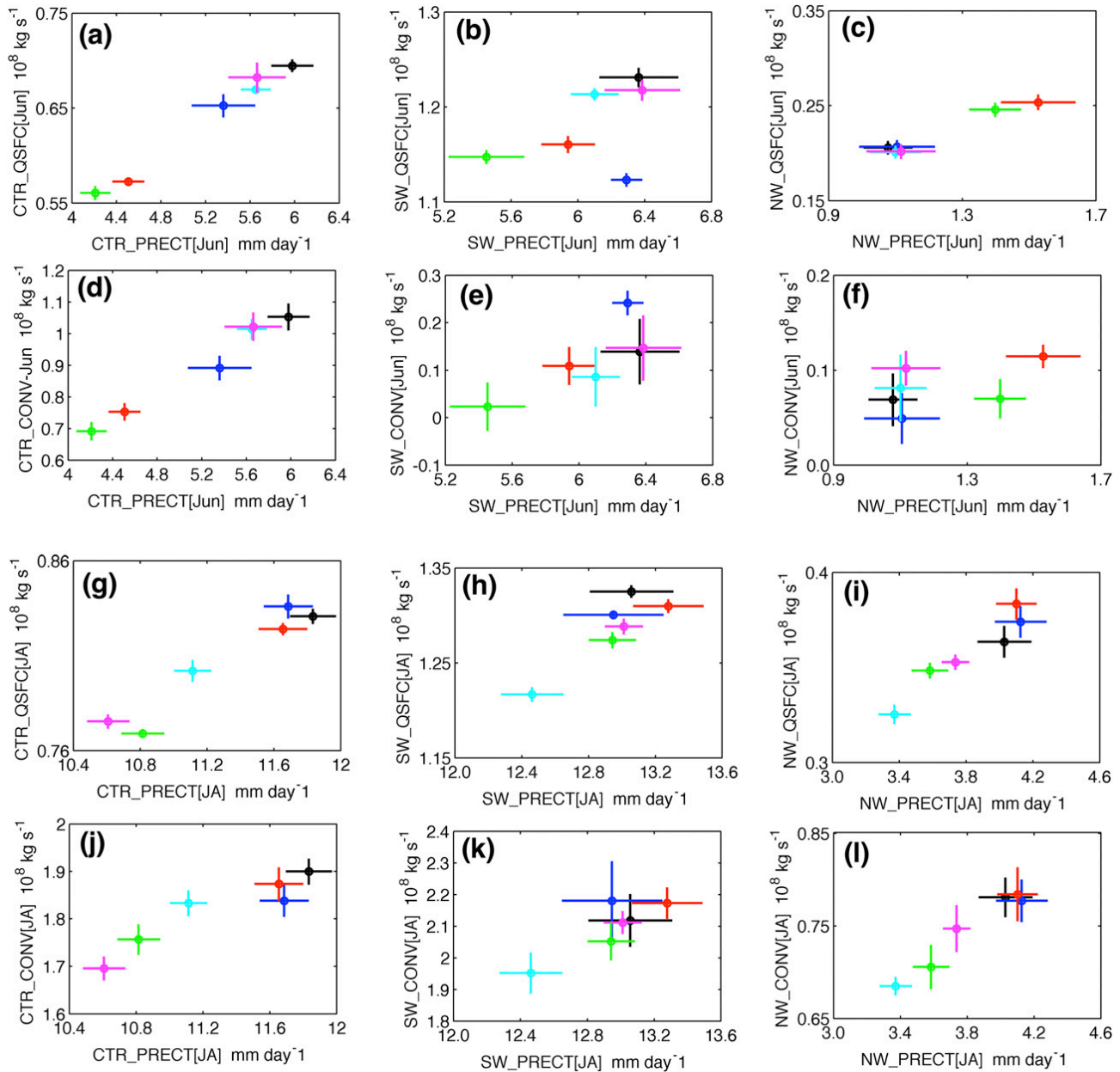
FIG. 8. As in Fig. 7, but showing subregional precipitation, surface water flux, and horizontal convergence of water vapor flux. (a)–(c) QSFC[Jun] vs PRECT[Jun] for the central (CTR), southwestern (SW), and northwestern (NW) India regions, respectively. (d)–(f) QCONV[Jun] vs PRECT[Jun] for the CTR, SW, and NW regions, respectively. (g)–(l) As in (a)–(f), but for JA. Note that tick marks are the same in all plots although the ranges are different.

Fig. 5k) and retained into the next season (Fig. 5d versus Fig. 5g).

5. Interannual variability

The CESM as run under perpetual year-2000 forcing displays its own internal variability (see appendix, section c). One such interannual variability is a Pacific mode similar to El Niño–Southern Oscillation (ENSO).

This model of ENSO is generally well represented in simulations either forced with prescribed SST (Meehl et al. 2012) or coupled with an ocean model (Deser et al. 2012), although its strength does not normally match observations. Less well captured is the relationship between ENSO and the following South Asian summer monsoon. In phases 3 and 5 of the Coupled Model Intercomparison Project (CMIP) experiments, the modeled ENSO has been found to exert excessive

TABLE 4. As in Tables 1–3, but showing changes of the monsoon diagnostics in the forced simulations from the control simulation, during the year succeeding warm, neutral, and cool years with regard to modeled ENSO. In the second column, the top and bottom cell of each diagnostic show how the diagnostic in warm-succeeding and cool-succeeding years compares with neutral-succeeding years (middle). When the *p* level is between 0.10 and 0.15, the change is written as [*I*: *x*] and [*D*: *x*] for increase and decrease from the control at *p* level of *x*, respectively.

Diagnostic	Premonsoonal forcing			Monsoonal forcing	
	BOCEANHF-PRE	BMODELHF-PRE	BMODELHF-BOTH	BMODELHF-MON	BOCEANHF-MON
a			*Decrease*		*Decrease*
JETSTR[JA]			*Decrease*		*
More	*Decrease*	*Increase*		**Decrease**	
b				*Decrease*	**Decrease**
ALL_PRECT[JA]			**Decrease**	*Decrease*	Decrease
Less	*Increase*	**Increase**	*Increase*		
c	*Decrease*		Decrease	**Decrease**	Decrease
CTR_PRECT[JA]		*Decrease*	**Decrease**	**Decrease**	**Decrease**
	Decrease		Decrease	**Decrease**	
d	[*D*: 0.14]		[*D*: 0.13]		Decrease
SW_PRECT[JA]				*	*
	[*I*: 0.14]	Increase	[*I*: 0.14]	[*I*: 0.14]	
e *Less*			*Decrease*	[*D*: 0.13]	**Decrease**
NW_PRECT[JA]			*Decrease*	Decrease	**Decrease**
More	Increase	*Increase*	[*I*: 0.14]	*Increase*	

influence on the following summer monsoon in comparison to observations (Jourdain et al. 2013).

The results of our control simulation (B2000NOAER) show the expected decrease in all-India monsoon precipitation during the summer preceding warm-phase or El Niño–like years (not shown). However, the expected increase in precipitation during the succeeding summer (i.e., the delayed ENSO effect; Webster et al. 1998) was not found in the simulation, although cool-succeeding years were indeed drier as expected (Table 4). In addition, certain actual physical processes (e.g., Park et al. 2010) may not be accurately represented in the model. Therefore, we will only briefly discuss the interannual variability of the model below rather than do a detailed analysis that may not accurately reflect reality.

The analysis in section 3 was repeated for the summer monsoon season preceding and succeeding warm and cold modeled ENSO years and compared to that of neutral-succeeding years. Using this method, we find no obvious differences in the preceding season between warm and cold years, as well as during June of the succeeding season. However, July–August precipitation responses succeeding warm and cold years are found of opposing directions.

Referring to row b of Table 4, neutral-succeeding years show changes consistent with results from the climatology—only simulations forced during the monsoonal period showed statistically significant changes (reduction) in July–August all-India precipitation. Warm-succeeding and cold-succeeding years show a different pattern. In the three simulations with premonsoonal aerosol

forcing (BOCEANHF-PRE, BMODELHF-PRE, and BMODELHF-BOTH), July–August precipitation was not significantly changed during warm-succeeding years but significantly increased during cold-succeeding years. In the two simulations forced by aerosol forcing only during the monsoonal period (BOCEANHF-MON and BMODELHF-MON), July–August precipitation during warm-succeeding years was significantly decreased but not significantly changed during the cold-succeeding years.

The regional precipitation contribution responsible for the difference between warm-succeeding and cold-succeeding years was in large part from northwestern India and to a lesser extent from southwestern India (Table 4, rows d and e). Over northwestern India, the perturbed simulations were drier in general during warm-succeeding and wetter during cold-succeeding years; both were in the same direction of variation as reflected in the control simulation for warm-succeeding or cold-succeeding years, respectively. Thus, the overall effect of aerosol forcing is to amplify the interannual variability of precipitation over northwestern India in the model.

Finally, we note that in cold-succeeding years, realistic premonsoonal forcing could strengthen the monsoon jet transport of water vapor during June (Table 4, row a). In these years, precipitation increase over southwestern India was statistically significant at the 95% confidence level (Table 4, row d). Since the southwest subregion formed the largest contribution to the three-region total (Figs. 7f–h), this together with the precipitation increase

over northwestern India (Table 4, row e) resulted in a strong signal of increased all-India precipitation statistically significant at the 99% confidence level. Increased all-India precipitation during cold-succeeding years is statistically significant when monsoonal-period forcing is included in the realistic simulation (BMODELHF-BOTH; Table 4, row b) but only at the 90% confidence level.

Thus, climatological results of the precipitation response to aerosol forcing might depend on the choice of years used to calculate the climatology and the multidecadal activity (warm tending or cold tending) during that period. Detecting and attributing increased interannual variance in rainfall over northwest and southwestern India would, however, be practically very difficult.

6. Discussion and conclusions

This study employs sensitivity tests to address two remaining issues regarding the direct radiative effect of anthropogenic absorbing aerosols on the South Asian summer monsoon climate: first, the respective roles of aerosol forcing before and after monsoon onset, as well as their interaction, and second, the sensitivity of the summer monsoon response to the spatial distribution of aerosol forcing, particularly premonsoonal forcing.

Using the CESM with fully coupled dynamical configuration of all component models, five simulations perturbed by different prescribed shortwave forcing were compared to the control simulation of year 2000, all with natural aerosols removed. The precipitation response of the South Asian monsoon was analyzed during the premonsoonal onset period (June) and the monsoon-established period (July–August) and for three subregions of India: central, southwest, and northwest. The northeastern subregion is excluded in discussion because precipitation over that subregion is not well captured by the model.

We first conducted a set of three simulations using realistic aerosol forcing prescribed based on a previous study using an interactive aerosol model, exerted respectively during the premonsoonal period, the monsoonal period, and throughout both periods. This set is used to examine the effectiveness of absorbing aerosol radiative forcing applied during different stages in causing climate responses of the monsoon and the interaction between these responses.

In response to realistic premonsoonal forcing, June precipitation decreases over central and southwestern India but increases over northwestern India, while the large-scale monsoon circulation is weakened—a result consistent with previous findings. Interestingly, we find that the response to this premonsoonal forcing remains through July–August specifically over central India, where a statistically significant drying with nearly no perturbation to the large-scale monsoon circulation has been identified after monsoon onset and also disappearance of prescribed aerosol forcing. This drying is found to be primarily caused by reduced soil water retaining the effect of June dryness into the succeeding months (Fig. 9) instead of through ocean heat storage. While ocean heat storage exists as well, the mechanism is found to be strong only when aerosol forcing persists past monsoon onset.

Realistic forcing during the monsoonal period alone, without forcing during the premonsoonal period, reduces July–August precipitation over all three analyzed subregions of India. This is primarily a localized effect, since there is no significant change in the strength of the large-scale monsoon circulation. However, the monsoon jet rotates to a more east–west orientation, likely contributing to drying over northwestern India.

When forcing is prescribed throughout both premonsoonal and monsoonal periods, changes in the July–August climate remain similar to those caused by monsoonal-period-only forcing, only stronger. Unlike in the simulations with forcing only during either the premonsoon or monsoon period, the large-scale monsoon circulation is significantly weakened during July–August because aerosol forcing persists through both periods. The propagation of perturbations by premonsoonal aerosols into the monsoonal period has been thought to be due to the high inertia of the oceanic system. At the same time, the longer time scale of ocean–atmosphere interaction also means that perturbing the oceanic system through the aerosol radiative effect is more effective when the forcing is sustained past the premonsoonal period into the monsoonal period. However, aerosol forcing during winter was not included in the simulation. In reality, aerosol forcing during these months would contribute to the longer forcing period required to perturb the oceanic system, such that the monsoonal forcing period is less important for this purpose.

Aerosol forcing during the monsoonal period is relatively weaker than in the premonsoonal period because of precipitation scavenging. However, other factors, including advective sources of water vapor as well as geographic characteristics, change from the premonsoonal to the monsoonal period as well. We find that July–August drying over central India can be explained by a localized aerosol cooling effect at the surface. For the July–August drying over northwestern India, the perturbation of the large-scale circulation in the form of a rotation of the monsoon jet to a more zonal orientation appears to be more important than the localized effect. Notably, both result from the weaker aerosol forcing in the monsoonal period.
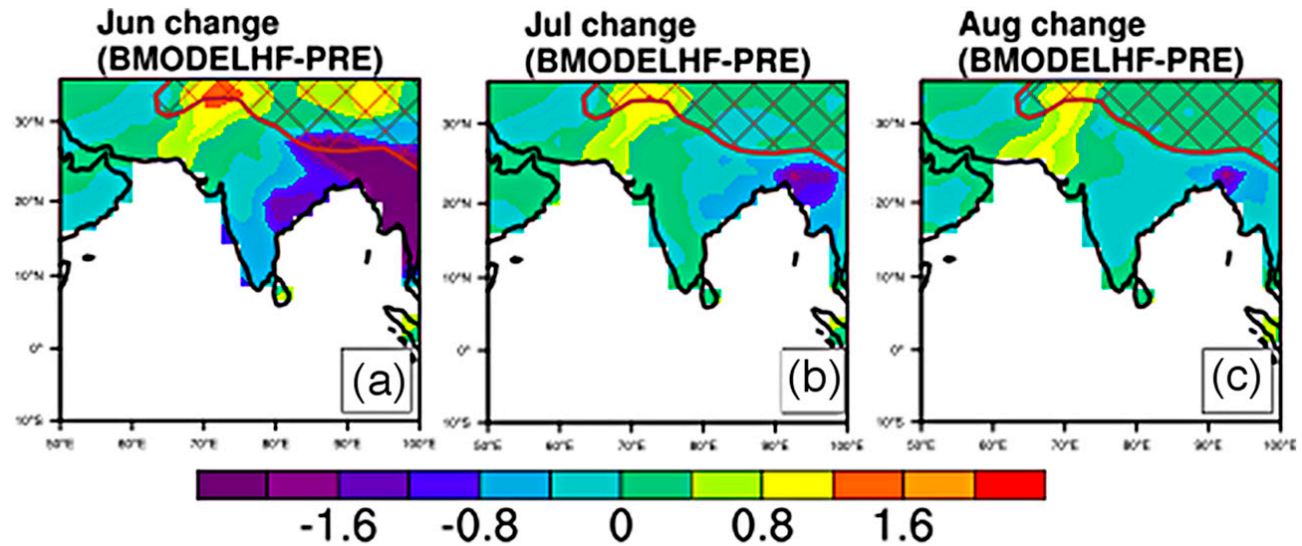
FIG. 9. As in Fig. 5, but showing changes in the soil water vertically integrated over the first 1 m of soil (cm) during (a) June, (b) July, and (c) August.

Aerosol forcing through both premonsoonal and monsoonal periods can also induce a rotation of monsoon jet in June to a more meridional orientation. The jet rotation acts to increase the water vapor flux northward, working against the overall weakening of the monsoon. If only the meridional direction is considered in this region, there is an increased northward transport of water vapor by the monsoon jet and a wetting over northwestern India.

We have also conducted simulations using a wide-area "cloud like" forcing and compared the results with those from simulations using the realistic forcing. The difference between the two types of distributions allows us to examine the sensitivity of monsoon response to aerosol forcing over the ocean, in particular over the Arabian Sea.

Drying over central India during the month of June is found to be insensitive to aerosol forcing distributions in the premonsoonal period, and the drying occurs regardless of whether the monsoon jet strengthens or weakens. On the other hand, precipitation over northwestern and southwestern India is not significantly changed when the premonsoonal aerosol forcing is wide area but increases and decreases, respectively, when the forcing is realistic. Thus, the presence or absence of precipitation signals over northwestern and southwestern India in past studies could be due to discrepancies in the aerosol spatial distribution used.

Finally, model results suggest that more investigation into aerosol-induced rainfall variability is warranted in the future. The model exhibits a mode of ENSO-like interannual variability. Given the same aerosol radiative forcing, climate responses in July–August display an interannual variation as well, succeeding warm and cold phases of the modeled ENSO. In the control simulation itself, warm-succeeding seasons are drier than cold-succeeding seasons over northwest India. Warm-succeeding seasons are found to be drier in the forced simulations compared to the control simulation, while cold-succeeding seasons are wetter compared to the control over northwestern India and to a lesser extent southwestern India. Therefore, aerosol forcing acts to increase precipitation variability over northwest and southwest India. However, the model representation of monsoon internal variability is still imperfect, and this signal is weak in the most realistic simulation.

APPENDIX

Model Diagnostics

a. Monsoon-representative variables

Diagnostic quantities have been defined to describe certain characteristics of the South Asian monsoon and

TABLE A1. The labels of the simulations performed, description of the simulations, and the number of years of integration.

Simulation	Description	No. years
B2000NOAER	Control simulation with no aerosol forcing.	240
BMODELHF-PRE	Realistic forcing from April to June (Figs. 1d–f).	240
BMODELHF-MON	Realistic forcing from July to September (Figs. 1g–i).	240
BMODELHF-BOTH	Realistic forcing from April to September (Figs. 1d–i).	240
BOCEANHF-PRE	Idealized wide-area forcing of transported aerosol from May to June (Figs. 1a,b).	200
BOCEANHF-MON	Idealized wide-area forcing of transported aerosol from July to August (Figs. 1a,b).	200

to reflect the regional changes of the monsoon system under aerosol forcing (Table A1). The diagnostics are summarized in Table A2, and the details are described below.

NW_PRECT, SW_PRECT, and CTR_PRECT are the monthly mean total precipitation averaged over northwestern India (25°–35°N, 65°–75°E), southwestern India (5°–10°N, 65°–75°E), and central India (15°–25°N, 75°–85°E), respectively, shown as red boxes in Fig. A1b. The monthly mean total precipitation averaged over all three regions together is named ALL_PRECT. Northeastern India is not analyzed because the regional precipitation was not well represented by the model. The box defined as southwestern India covers a large portion of the ocean in order to capture the precipitation pattern in the global model. This is because much of the precipitation over the southwest region falls over the ocean in the model instead of coastal inland as observed. We assume that the precipitation maximum over the ocean in the model represents the coastal precipitation maximum in observations. May is excluded in the diagnostics because the rainfall pattern during May resembles the rainfall pattern of the winter monsoon months more than the

rainfall pattern during June and throughout the rest of the summer monsoon season.

JETSTR is the monthly mean water vapor flux, vertically integrated in the lowest 7 model levels (i.e., from the surface up to ~570 hPa) and taking the spatial mean of that quantity over the region of 5°–10°N, 50°–65°E (Fig. A1c). This region is the location of the lower-tropospheric westerly monsoon jet, and the diagnostic is a measure of the strength of the large-scale monsoon circulation. JETANG is the angle the mean water vapor flux vector makes with the north, referring to the direction the wind vector points toward. The diagnostics are calculated for June and from July to August. The month of May is not included because the summer monsoon circulation is not yet established in May.

The onset of the summer monsoon with the northward movement of the tropical convergence zone follows the evolution of the meridional temperature gradient, which we measure with TSDIFF, defined as the difference of the monthly mean skin temperature between the regions of 5°–25°N, 60°–100°E and 20°S–0°, 60°–100°E (Fig. A1a). These are the same regions used by Ramanathan et al. (2005) to calculate the meridional temperature gradient. The diagnostic is calculated from

TABLE A2. Derived diagnostic variables from model output. See Table 1 for the period for which a variable is calculated.

| Variable	Description
TSDIFF	The difference of the monthly mean skin temperature between the regions 5°–25°N, 60°–100°E and 20°S–0°, 60°–100°E.
JETSTR	The magnitude of the monthly mean vertically integrated water vapor flux of the lowest 7 model levels (i.e., the lower troposphere up to ~570 hPa) in the region 5°–20°N, 50°–65°E.
JETANG	The angle from north of the monthly mean vertically integrated water vapor flux of the lowest 7 model levels in the region 5°–20°N, 50°–65°E.
ALL_PRECT	The monthly mean total precipitation in northwestern India, southwestern India, and central India as defined below.
NW_PRECT	The monthly mean total precipitation in northwestern India, defined as the region 25°–35°N, 65°–75°E.
SW_PRECT	The monthly mean total precipitation in southwestern India, defined as the region 5°–20°N, 65°–75°E.
CTR_PRECT	The monthly mean total precipitation in central India, defined as the region 15°–25°N, 75°–85°E.
NW_QCONV SW_QCOV CTR_QCONV	The convergence of the monthly mean horizontal water vapor flux in the lower troposphere up to approximately 570 hPa, over the three subregions defined above.
NW_QSFC SW_QSFC CTR_QSFC	The monthly mean surface water flux over the three subregions defined above (from the atmospheric model component).
H2OSOI	The monthly mean column-integrated soil water in the top 1 m (from the land model component).
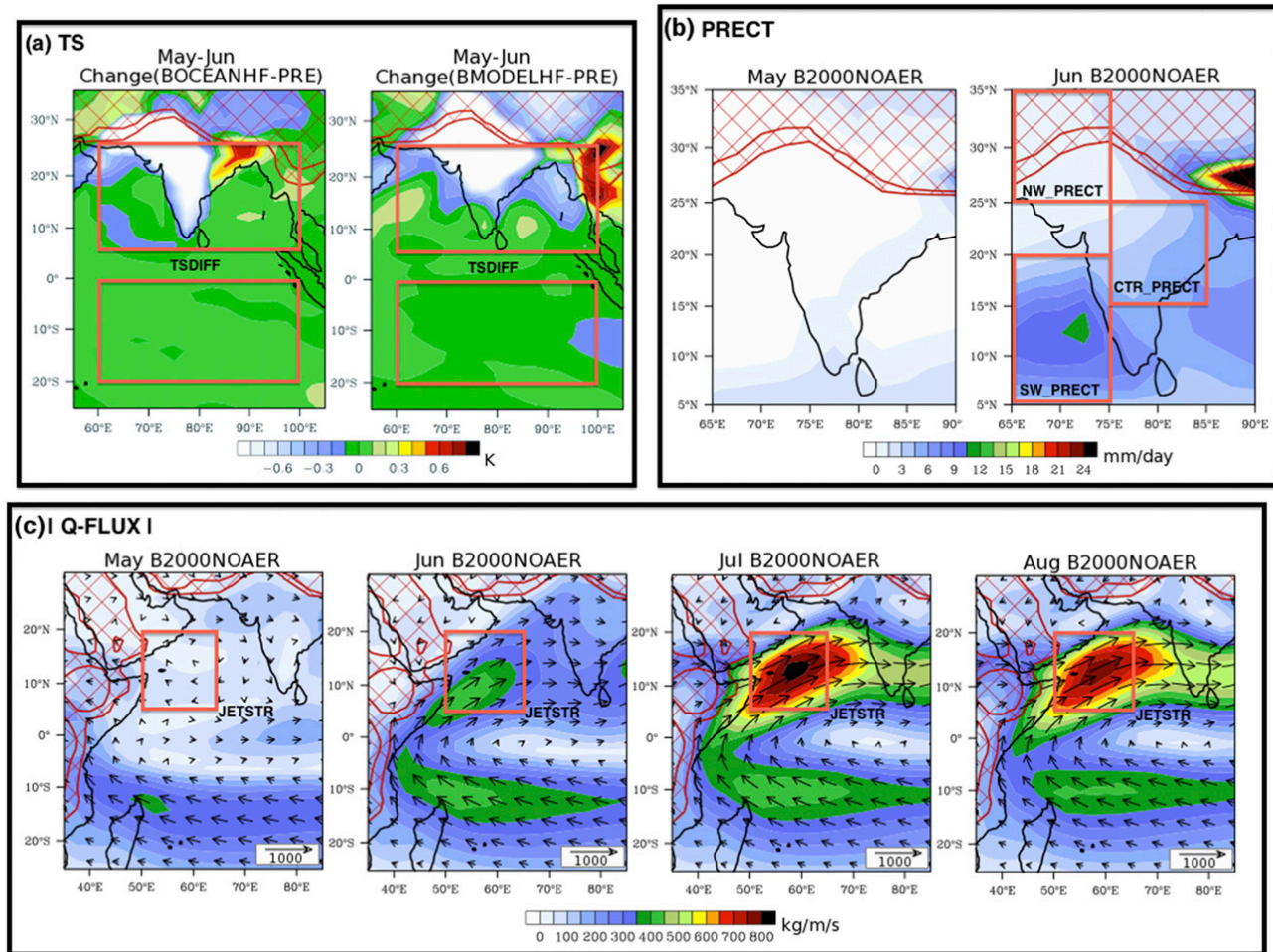
FIG. A1. (a) Red boxes show the two regions used for the calculation of TSDIFF. (b) Red boxes show the subregions of India used for the calculation of the precipitation diagnostics NW_PRECT, CTR_PRECT, and SW_PRECT. (c) Red boxes show the region used for the calculation of JETSTR and JETANG.

May to June, with the motivation of understanding how changes in the interhemispheric temperature difference—measuring the meridional temperature gradient—impact the strength of the monsoon circulation. May values are still retained in the calculation of TSDIFF because it is possible for May temperature patterns over the region to influence the June circulation because of the heat storage in the ocean. In preliminary analysis, the diagnostic for the period of July to August is found to have a strong dependence on land precipitation. This quantity is not used in this manuscript.

b. Statistical tests

When performing the analysis, the first 100 years of all model simulations have been discarded to avoid the period with transient character. To produce a population of "climates" for each simulation, the remaining years were grouped into consecutive periods of 20 years each. The mean diagnostics of each group were calculated to form relatively independent samples of climates. The distributions of the climate diagnostics have been tested for normality using the nonparametric Kolmogorov–Smirnov test. As many distributions failed normality, we use the Kolmogorov–Smirnov test to compare between the diagnostic populations of the forcing simulations and the control simulation. The 90% confidence level is used as the criteria for statistical significance.

c. Interannual variability

To extract the populations of Pacific Ocean variability in warm, neutral, or cool phase, the first and last year of the remaining years after 100 years have been discarded and each summer classified by a Niño-3.4-like index of the preceding December, January, and February (DJF). This is the anomaly from the climatic annual cycle of the mean skin temperature over the region enclosed by 120°–170°W and 5°S–5°N. A particular summer is

considered to be phase warm or cool transitioning if the mean preceding DJF index exceeds or falls below one standard deviation of the climatic mean index value, respectively, and phase neutral otherwise.

We assume that the prescribed radiative forcing in the perturbed simulations is small enough such that changes in the Pacific interannual mode are also small. This assumption is supported by the result that the fraction of phase-warm and phase-cool years remains about the same in all the simulations—approximately one-quarter phase-warm years, one-quarter phase-cool years, and the rest phase-neutral years. Note that the exact years considered phase warm or phase cool are different for each simulation.

REFERENCES

Bollasina, M. A., Y. Ming, and V. Ramaswamy, 2011: Anthropogenic aerosols and the weakening of the South Asian summer monsoon. *Science,* **334,** 502–505, doi:10.1126/science.1204994.

Chung, C. E., and V. Ramanathan, 2006: Weakening of the north Indian SST gradients and the monsoon rainfall in India and the Sahel. *J. Climate,* **19,** 2036–2045, doi:10.1175/JCLI3820.1.

——, ——, and J. T. Kiehl, 2002: Effects of the South Asian absorbing haze on the northeast monsoon and surface–air heat exchange. *J. Climate,* **15,** 2462–2476, doi:10.1175/1520-0442(2002)015<2462:EOTSAA>2.0.CO;2.

Collier, J. C., and G. J. Zhang, 2009: Aerosol direct forcing of the summer Indian monsoon as simulated by the NCAR CAM3. *Climate Dyn.,* **32,** 313–332, doi:10.1007/s00382-008-0464-9.

Deser, C., and Coauthors, 2012: ENSO and Pacific decadal variability in the Community Climate System Model version 4. *J. Climate,* **25,** 2622–2651, doi:10.1175/JCLI-D-11-00301.1.

Ganguly, D., P. J. Rasch, H. Wang, and J.-H. Yoon, 2012a: Fast and slow responses of the South Asian monsoon system to anthropogenic aerosols. *Geophys. Res. Lett.,* **39,** L18804, doi:10.1029/2012GL053043.

——, ——, ——, and ——, 2012b: Climate response of the South Asian monsoon system to anthropogenic aerosols. *J. Geophys. Res.,* **117,** D13209, doi:10.1029/2012JD017508.

Gent, P. R., and Coauthors, 2011: The Community Climate System Model version 4. *J. Climate,* **24,** 4973–4991, doi:10.1175/2011JCLI4083.1.

Jourdain, N. C., A. Sen Gupta, A. S. Taschetto, C. C. Ummenhofer, A. F. Moise, K. Ashok, 2013: The Indo-Australian monsoon and its relationship to ENSO and IOD in reanalysis data and the CMIP3/CMIP5 simulations. *Climate Dyn.,* **41,** 3073–3102, doi:10.1007/s00382-013-1676-1.

Kim, D., C. Wang, A. M. L. Ekman, M. C. Barth, and P. Rasch, 2008: Distribution and direct radiative forcing of carbonaceous and sulfate aerosols in an interactive size-resolving aerosol–climate model. *J. Geophys. Res.,* **113,** D16309, doi:10.1029/2007JD009756.

Lau, K. M., and K. M. Kim, 2007: Does aerosol weaken or strengthen the Asian monsoon? *Mountains, Witnesses of Global Changes,* R. Baudo et al., Eds., Elsevier, 13–22.

——, and ——, 2010: Fingerprinting the impacts of aerosols on long-term trends of the Indian summer monsoon regional rainfall. *Geophys. Res. Lett.,* **37,** L16705, doi:10.1029/2010GL043255.

——, M. K. Kim, and K. M. Kim, 2006: Asian summer monsoon anomalies induced by aerosol direct forcing: The role of the Tibetan Plateau. *Climate Dyn.,* **26,** 855–864, doi:10.1007/s00382-006-0114-z.

Lee, S.-Y., H.-J. Shin, and C. Wang, 2013: Nonlinear effects of coexisting surface and atmospheric forcing by anthropogenic absorbing aerosols: Impact on the South Asian monsoon onset. *J. Climate,* **26,** 5594–5607, doi:10.1175/JCLI-D-12-00741.1.

Meehl, G. A., J. M. Arblaster, and W. D. Collins, 2008: Effects of black carbon aerosols on the Indian monsoon. *J. Climate,* **21,** 2869–2882, doi:10.1175/2007JCLI1777.1.

——, ——, J. Caron, H. Annamalai, M. Jochum, A. Chakraborty, and R. Murtugudde, 2012: Monsoon regimes and processes in CCSM4. Part 1: The Asian–Australian monsoon. *J. Climate,* **25,** 2583–2608, doi:10.1175/JCLI-D-11-00184.1.

Menon, S., J. Hansen, L. Nazarenko, and Y. Luo, 2002: Climate effects of black carbon aerosols in China and India. *Science,* **297,** 2250–2253, doi:10.1126/science.1075159.

Ming, Y., V. Ramaswamy, P. A. Ginoux, and L. H. Horowitz, 2005: Direct radiative forcing of anthropogenic organic aerosol. *J. Geophys. Res.,* **110,** D20208, doi:10.1029/2004JD005573.

Park, H. S., J. C. Chiang, B. R. Lintner, and G. J. Zhang, 2010: The delayed effect of major El Niño events on Indian monsoon rainfall. *J. Climate,* **23,** 932–946, doi:10.1175/2009JCLI2916.1.

Ramanathan, V., and Coauthors, 2001: Indian Ocean Experiment: An integrated analysis of the climate forcing and effects of the great Indo-Asian haze. *J. Geophys. Res.,* **106,** 28 371–28 398, doi:10.1029/2001JD900133.

——, and Coauthors, 2005: Atmospheric brown clouds: Impacts on South Asian climate and hydrological cycle. *Proc. Natl. Acad. Sci. USA,* **102,** 5326–5333, doi:10.1073/pnas.0500656102.

Randles, C. A., and V. Ramaswamy, 2008: Absorbing aerosols over Asia: A Geophysical Fluid Dynamics Laboratory general circulation model sensitivity study of model response to aerosol optical depth and aerosol absorption. *J. Geophys. Res.,* **113,** D21203, doi:10.1029/2008JD010140.

Wang, C., 2004: A modeling study on the climate impacts of black carbon aerosols. *J. Geophys. Res.,* **109,** D03106, doi:10.1029/2003JD004084.

——, 2007: Impact of direct radiative forcing of black carbon aerosols on tropical convective precipitation. *Geophys. Res. Lett.,* **34,** L05709, doi:10.1029/2006GL028416.

——, G.-R. Jeong, and N. Mahowald, 2009a: Particulate absorption of solar radiation: Anthropogenic aerosols vs. dust. *Atmos. Chem. Phys.,* **9,** 3935–3945, doi:10.5194/acp-9-3935-2009.

——, D. Kim, A. M. L. Ekman, M. C. Barth, and P. J. Rasch, 2009b: Impact of anthropogenic aerosols on Indian summer monsoon. *Geophys. Res. Lett.,* **36,** L21704, doi:10.1029/2009GL040114.

Webster, P. J., V. O. Magaña, T. N. Palmer, J. Shukla, R. A. Tomas, M. Yanai, and T. Yasunari, 1998: Monsoons: Processes, predictability, and the prospects for prediction. *J. Geophys. Res.,* **103** (C7), 14 451–14 510, doi:10.1029/97JC02719.

The MIT Joint Program on the Science and Policy of Global Change combines cutting-edge scientific research with independent policy analysis to provide a solid foundation for the public and private decisions needed to mitigate and adapt to unavoidable global environmental changes. Being data-driven, the Program uses extensive Earth system and economic data and models to produce quantitative analysis and predictions of the risks of climate change and the challenges of limiting human influence on the environment—essential knowledge for the international dialogue toward a global response to climate change.

To this end, the Program brings together an interdisciplinary group from two established MIT research centers: the Center for Global Change Science (CGCS) and the Center for Energy and Environmental Policy Research (CEEPR). These two centers—along with collaborators from the Marine Biology Laboratory (MBL) at Woods Hole and short- and long-term visitors—provide the united vision needed to solve global challenges.

At the heart of much of the Program's work lies MIT's Integrated Global System Model. Through this integrated model, the Program seeks to: discover new interactions among natural and human climate system components; objectively assess uncertainty in economic and climate projections; critically and quantitatively analyze environmental management and policy proposals; understand complex connections among the many forces that will shape our future; and improve methods to model, monitor and verify greenhouse gas emissions and climatic impacts.

This reprint is one of a series intended to communicate research results and improve public understanding of global environment and energy challenges, thereby contributing to informed debate about climate change and the economic and social implications of policy alternatives.

Ronald G. Prinn and John M. Reilly,
Program Co-Directors

For more information, contact the Program office:
MIT Joint Program on the Science and Policy of Global Change

Postal Address:
Massachusetts Institute of Technology
77 Massachusetts Avenue, E19-411
Cambridge, MA 02139 (USA)

Location:
Building E19, Room 411
400 Main Street, Cambridge

Access:
Tel: (617) 253-7492
Fax: (617) 253-9845
Email: ***globalchange@mit.edu***
Website: ***http://globalchange.mit.edu/***